Environmental Research Communications

LETTER

Temporal and spatial patterns of heat extremes in Hesse, Germany

S Krikau and S A Benz

Institute of Photogrammetry and Remote Sensing, Karlsruhe Institute of Technology, Karlsruhe, Germany

E-mail: krikau@kit.edu

OPEN ACCESS

RECEIVED
13 January 2025

REVISED
28 March 2025

ACCEPTED FOR PUBLICATION
17 April 2025

PUBLISHED
2 May 2025

Keywords: land surface temperature (LST), thermal comfort, temperature anomaly, (surface) urban heat island (UHI), heat stress, heat extreme, urban-rural intensity differences

Supplementary material for this article is available online

Abstract

Elevated temperatures due to the Urban Heat Island (UHI) effect, combined with a high population density, increase the risk of heat-related illnesses in urban areas. Spatial data on heat stress is crucial for effective mitigation strategies in urban planning. However, meteorological parameters like air temperature (Ta) and relative humidity (RH), necessary for thermal comfort indices such as Physiological Equivalent Temperature (PET) and Humidex, are often unavailable at fine spatial resolutions. Consequently, Land Surface Temperature (LST) from spaceborne thermal sensors are commonly used as a substitute. Here we evaluate the spatial and temporal patterns of LST, Ta, PET, and Humidex by analysing urban-rural intensity differences (ΔT) in Hesse, Germany, at a 1 km resolution. The Humidex (max: 4.3 °C) dataset reveals an amplified UHI effect compared to Ta (max: 2.9 °C) and LST (max: 3.4 °C), suggesting that relying solely on LST or Ta may underestimate heat stress. While LST is often used to approximate Ta, there is high correlation to thermal comfort indices such as PET during the day ($r = 0.49$) and ΔHumidex ($r = 0.47$) at night.

1. Introduction

Heat poses a major risk to human health and ecosystems, especially during extreme heat events (Semenza *et al* 1996; Yadav *et al* 2023). It causes health conditions such as dehydration, heat exhaustion and heatstroke (Hajat *et al* 2010, Stone *et al* 2023). The increase in global temperatures as a consequence of climate change is anticipated to exacerbate extreme heat events (Meehl and Tebaldi 2004, IPCC 2023) and thermal hazards (Mora *et al* 2017, Raymond *et al* 2020). Urban populations are particularly susceptible to these alterations due to their high population density and the Urban Heat Island (UHI) effect, characterized by elevated temperatures relative to their adjacent rural areas (Oke 1973). To combat this hazard, targeted actions are needed through urban planning and public health interventions (Mavrakou *et al* 2018). However the scarcity of meteorological measurement stations, even with the inclusion of portable and mobile sensors (Speak and Salbitano 2022), fail to capture the spatial variability of thermal conditions within cities. This limitation results in an incomplete understanding of urban thermal comfort and emphasizes the need for a comprehensive evaluation of available parametrization of heat extremes at scale.

Utilizing satellite imagery to estimate Land Surface Temperature (LST) offers high spatial coverage, including regions without ground-based measurement stations. During the last decade, these data sources have been frequently used for Surface UHI (SUHI) studies (Diem *et al* 2024, Pena Acosta *et al* 2023, Sismanidis *et al* 2023, Karimi *et al* 2021, Lin *et al* 2024, Chakraborty and Lee 2019) even though their relationship to how humans experience heat on a local scale has been challenged (Patel *et al* 2024, Venter *et al* 2021), since LST and air temperature (Ta) represent different thermal measures of the environment and may not correlate well, especially during the day (Coutts *et al* 2016). To quantify the thermal conditions relevant for human well being in outdoor areas thermal comfort indices such as the universal Thermal Climate Index (UTCI) (Jendritzky and de Dear 2012) and the Physiologically Equivalent Temperature (PET) (Höppe 1999) have been introduced

(Blazejczyk *et al* 2012, Zare *et al* 2018, Migliari *et al* 2022). These indices depend on energy balance models alongside meteorological variables such as humidity, Ta, wind velocity, and both longwave and shortwave radiation, making them challenging and costly to assess accurately. As a result, they are often applied in localized studies (Kariminia *et al* 2016, Wallenberg *et al* 2023). Although meteorological reanalysis data such as the Reanalysis v5 by the European Centre for Medium-Range Weather Forecasts (ERA5) enable the calculation of thermal comfort indices like the UTCI (Di Napoli *et al* 2020) for a broad spatial and temporal range, urban areas remain under represented in this dataset (Nogueira *et al* 2022, Adinolfi *et al* 2023), leading to an underestimation of thermal stress. Other indices, such as the Humidex (Masterton and Richardson 1979), rely on a limited set of variables, making them more accessible and globally applied (Coccolo *et al* 2019, Wang *et al* 2023, Rød and Maarse 2021), although they were developed initially for specific regions and/or weather conditions. While the Humidex provides a straightforward method for evaluating heat stress, it does not account for the full heat budget and has a less direct correlation with UTCI compared to PET (Blazejczyk *et al* 2012).

The relationship between these different heat stress parameters remains a topic of ongoing discussion in the scientific community. Numerous studies have explored the impact of different land use/land cover (LULC) types, often characterized by indices like Normalized Difference Vegetation Index (NDVI) or Normalized Difference Built-up Index (NDBI), on LST, particularly in local urban environments (Fuladlu 2022, Imran *et al* 2022, Xu *et al* 2024, Naserikia *et al* 2023, Cetin *et al* 2024, Naserikia *et al* 2024), but also on cities at the global scale (Li *et al* 2023), with some studies focusing on urban-rural temperature anomalies (Benz *et al* 2021, Roy *et al* 2024). Beyond spatial variations, the temporal dynamics of LST have been explored in depth (Lai *et al* 2018, Stewart *et al* 2021). More recently, the introduction of Local Climate Zones (LCZs) (Demuzere *et al* 2022), a universal typology that distinguishes urban areas based on micro-scale land cover, building height, impervious surfaces, and thermal properties, has offered a more climate-relevant classification system compared to traditional LULC categorizations. By linking urban morphology with atmospheric responses, LCZs have provided new insights into urban heat dynamics and thermal comfort assessments. Despite extensive previous studies, there is still a lack of research that simultaneously examines thermal comfort, air temperature, and LST in relation to the urban heat island effect, while considering both temporal and regional spatial scales within the framework of LCZs.

Here we compare the different heat metrics by examining LST and Ta in relation to thermal comfort parameters such as PET and Humidex at a 1 km spatial resolution during summertime for the region of Hesse, Germany. The UHI effect quantifies the additional warming caused by urbanization, helping to isolate the impact of built environments on local microclimates. By focusing on urban-rural intensity differences (ΔT), which represent the deviation of local thermal parameters from rural background levels, we assess the urban impact while reducing the influence of broader climate patterns. This approach allows for a clearer understanding of how cities modify heat exposure. Diurnal and spatial patterns of temperature variations and thermal conditions are examined across different land use types and urban forms by incorporating the LCZ classification (Demuzere *et al* 2022). Using this approach, we aim to: a) determine whether urban-rural intensity differences based on thermal comfort indices (such as PET and Humidex) exhibit similar spatial and temporal patterns to those of ΔTa at a regional scale, and b) assess whether commonly available spatial datasets (such as LST) can serve as reliable proxies for estimating human-perceived heat stress across the LCZs, particularly in densely populated urban areas. We discuss the findings in the context of human thermal comfort, focusing on the vulnerability of urban populations and distinguishing between typical conditions and temperature extremes.

2. Materials and methods

2.1. Data selection

The study is conducted for the federal state of Hesse, Germany, which is part of two climate zones according to the Köppen-Geiger classification (Beck *et al* 2018, 2020). The northern area has a hilly terrain and a cold climate with warm summers, while the southern region, part of the Rhine Valley, has a predominantly flat terrain and a temperate climate influenced by the Mediterranean Sea (figures 1(h), (i)). Hesse is selected for its diverse environmental conditions and the availability of relevant data, although the methodology applied in this research can be adapted and implemented for any other area (within Germany).

At the beginning of 2024, the German Weather Service (DWD) published a new high-resolution hourly raster data set 'HOchaufgelöste STündliche RAsterDAtensatz' (HOSTRADA) (Krähenmann *et al* 2018), with a spatial resolution of 1 km^2 per raster grid cell. This dataset merges meteorological measurements from ground stations with satellite observations and model data for Germany starting from the year 1995. Urban process parameters are used so that the effect of UHIs can be adequately captured. Although full validation was not yet possible due to the limited number of measurement stations (Krähenmann *et al* 2018), we found marginal deviations when compared to urban meteorological stations from the 'CityClim' project (Karlsruhe 2024). Air

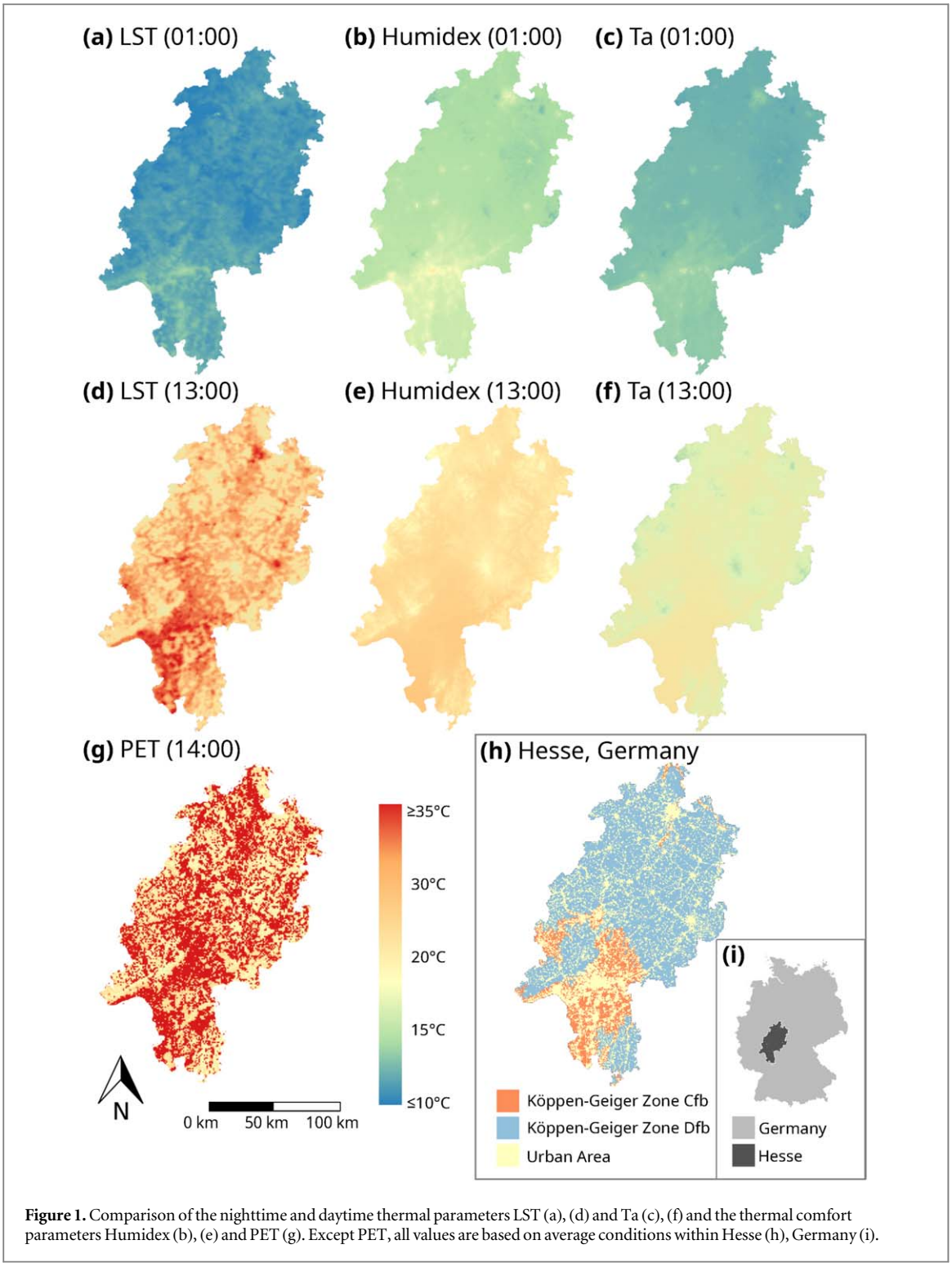

Figure 1. Comparison of the nighttime and daytime thermal parameters LST (a), (d) and Ta (c), (f) and the thermal comfort parameters Humidex (b), (e) and PET (g). Except PET, all values are based on average conditions within Hesse (h), Germany (i).

temperature (Ta) and relative humidity (RH) data is used from this data-collection for the summer months June, July, and August for the decade from 2011 to 2020. LST data is obtained from the MODerate-resolution Imaging Spectroradiometer (MODIS) on board of the Terra (Wan *et al* 2015) and Aqua (Wan *et al* 2021) satellites and preprocessed using Google Earth Engines Python API. Observations with uncertainties $\geqslant$3 Kelvin based on the information provided by the quality indicators *QC_Night* and *QC_Day* are not included during data aggregation. The research decade under investigation is selected based on the availability of census and land use/land cover datasets for a whole decade. Specifically, the census data (Ämter des Bundes and und der Länder 2011) from 2011, the CORINE Land Cover data (European Environment Agency 2020) from 2018 for the distinction between urban and rural areas and the Local Climate Zone (LCZ) dataset (Demuzere *et al* 2022) from 2018 is used.

To generate composite images of for the LST, Ta and Humidex datasets for the specific hours of the day during the research decade, both the mean values and the 90th percentile are calculated for each pixel $T(u, v)$ in the datasets. Since Crosson *et al* (2012) noted that MODIS Aqua data is more suited to sense the minimum and maximum surface temperature deviations, the corresponding full hours were selected for visualization purposes. The mean value provides information about the average temperature conditions (figures 1(a)–(f)), helping to understand general thermal patterns and typical thermal comfort, while the 90th percentile focuses on extreme temperatures.

2.2. Calculation of heat extreme events

Often certain temperature thresholds are used to assess heat stress and its impact on human well-being. Specifically, days with temperatures exceeding 30 °C (hot days) and 35 °C (very hot days) are critical markers in Germany (Deutsche Wetter Dienst 2025). For this analysis, the total number of such days over the entire study period is considered based on the HOSTRADA dataset. In addition to individual (very) hot days, prolonged periods of extreme heat (heat waves), are particularly relevant for assessing heat stress risks. A heat wave is defined here as a period of at least three consecutive days where temperatures exceed both the 95th percentile of the local temperature distribution and a minimum threshold of 28 °C. The number of heat wave events indicates how frequently such extreme periods occur, while the total number of heat wave days provides insight into the cumulative exposure to extreme heat over the analysed decade. The occurrence of extreme temperature events is highest in the south of Hesse (figure S4).

2.3. Thermal comfort indices

The thermal comfort index PET defined by Höppe (1999) and revised by Walther and Goestchel (2018) is derived from simulations by Ketterer *et al* (2022) using the 'Flow over Irregular Terrain with Natural and Anthropogenic Heat sources' (FITNAH) model for a a heat-intensive artificial day on an August 1st at 14:00. The meteorological conditions for the initial state are as follows: near-surface air temperature at 3:00 PM averages 29 °C, relative humidity is 20%, there is no prevailing (geostrophic) wind, and the sky is clear. Additional processing details can be found in Ketterer *et al* (2022). The original resolution of 200 m is reduced to 1 km using nearest neighbour resampling to align with the other datasets. PET uses a simplified thermoregulation model based on Fanger's model (as cited in Blazejczyk *et al* 2012), focusing on comfort in moderate conditions with less complexity regarding heat transfer between the body and the environment. Despite its simplified approach, compared to the UTCI, which incorporates a more complex multi-segment body model based on Fiala *et al* (2001), it is still one commonly used complex thermal comfort index in Germany. The Humidex (Masterton and Richardson 1979) is calculated via equation (1) (Tartarini and Schiavon 2020) using Ta and RH derived from the HOSTRADA dataset (figure 1). Since thermal comfort parameters are based on apparent temperatures, the temperature ranges for PET and Humidex vary across the stress categories (table S1).

$$\text{Humidex} = \mathrm{T_a} + \frac{5}{9} \cdot \left((6.112 \cdot 10^{\frac{7.5 \cdot \mathrm{T_a}}{237.7 + \mathrm{T_a}}}) \cdot \frac{\mathrm{RH}}{100} - 10 \right) \tag{1}$$

2.4. Calculation of urban-rural intensity differences

ΔT, in the literature referred to as temperature anomalies in the context of Ta or LST, are defined as differences between local and rural background air temperatures. Due to the extension to other thermal parameters we refer to them as urban-rural intensity differences. Based on the methodology developed by Benz *et al* (2021) for each pixel with a local temperature value $T(u, v)$ the median comparable rural background temperature $\bar{T}(u, v, r)_{\text{rural}}$ is subtracted (equation (2)). Comparable meaning within a 100 km radius r of the local pixel (therefore including pixel outside of Hesse when available) and with elevation differences of up to 100 m and similar slope aspects (north or south-facing). If more than 30 pixel are available, the median of these pixels is used to determine the comparable rural background temperature, otherwise, it is set as undefined. Positive anomalies above 0.5 °C indicate warmer conditions, while anomalies under −0.5 °C denote cooler conditions. By using this approach large-scale climate effects can be reduced and it ensures that temperature differences reflect urbanization effects rather than topographic variations.

$$\Delta T(u, v) = T(u, v)_{\text{local}} - \bar{T}(u, v, r)_{\text{rural}} \tag{2}$$

The calculation of urban-rural intensity differences for the thermal comfort dataset and other available thermal parameters is equally performed. While a stronger signal is expected due to the additional inclusion of RH, the following analysis will examine the relationship with LCZ, focusing on urban areas to refine our understanding. However, the PET dataset proved unsuitable for this approach, as the hotspots could not be clearly identified and did not show a clear pattern (figure S2), whereas the ΔHumidex dataset (min: −2.1 °C,

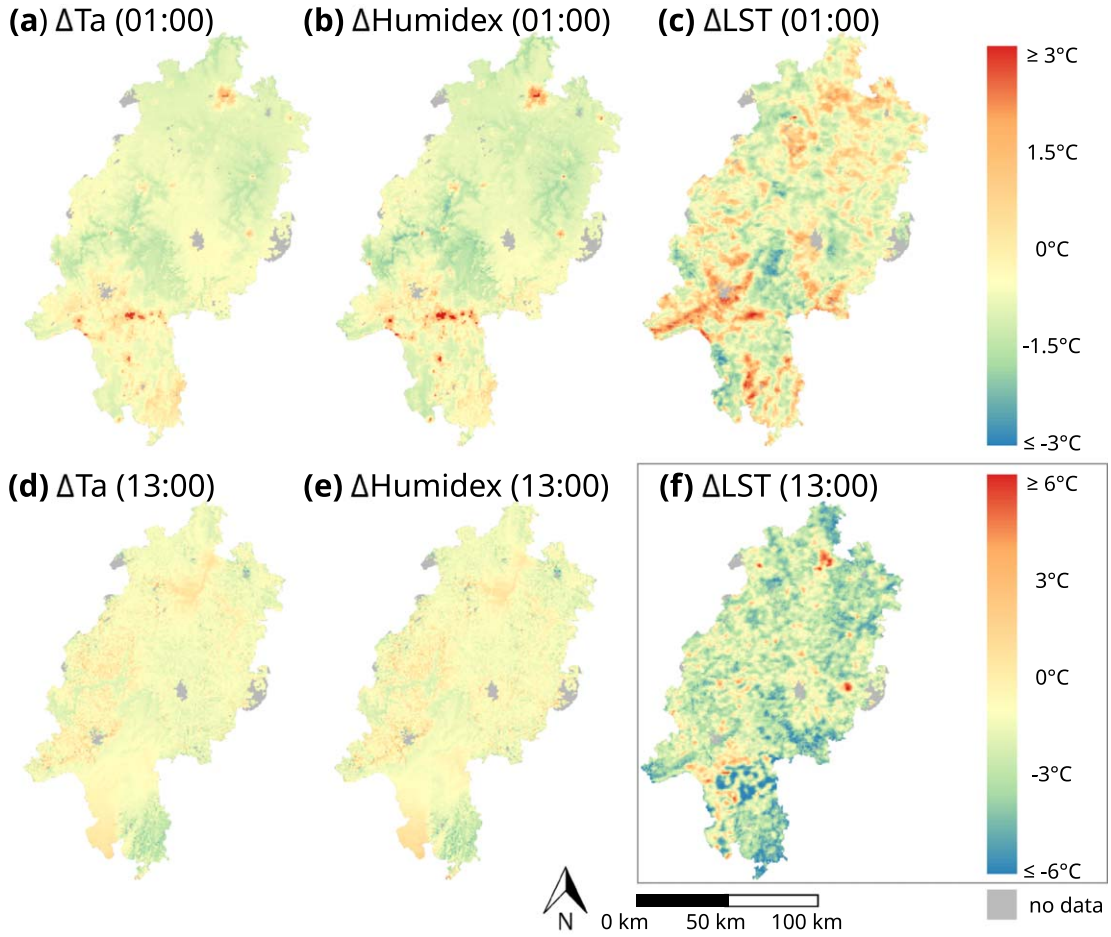

Figure 2. Nighttime and daytime urban-rural intensity differences based on Ta (a) and (d), Humidex (b), (e) and LST (c), (f). Urban areas can be over 3 °C warmer than the comparable rural background area.

max: 4.3 °C) is found to be effective, revealing an even stronger urban heat island effect compared to both ΔTa (min: −1.6 °C, max: 2.9 °C) and ΔLST (min: −3.0 °C, max: 3.4 °C) datasets (figure 2) for nighttime temperatures.

3. Results

3.1. Spatial variations under consideration of LCZs

Urban climate is influenced by the specific structural and surface characteristics categorized by the LCZ. Built types are in the classes 1 to 10 while land cover types are denoted alphabetical from A to G. In the region of Hesse, densely populated urban areas fall mainly into class 2 (compact mid-rise) and 5 (open mid-rise) (figure S1) and are particularly affected by elevated temperatures across all datasets (figure 3) during the nighttime at 01:00 hrs (min: −1.6 °C, max: 2.9 °C), when the UHI effect is most pronounced (Voogt and Oke 2003), and further magnified using the upper 90th percentile of Ta (min: −1.7 °C, max: 3.4 °C). With the inclusion of RH in the form of the Humidex the overall spatial pattern stays consistent, while the contrast between urban and rural areas is enhanced. The magnitude of positive urban-rural intensity differences are amplified, indicating that the urban population experiences higher stress levels than anticipated based on air temperature alone, although the total percentage of the population living in areas with positive urban-rural intensity differences during the daytime is reduced considering ΔHumidex instead of ΔTa. For the daytime the UHI effect is only evident in the ΔLST dataset, although the contrast between densely and sparsely populated areas is still most prominent during the nighttime. Thermal comfort values based on PET are generally homogeneously distributed across land cover zones but become increasingly inhomogeneous, with a tendency toward discomfort, in built-up areas at the 1 km spatial scale. However, this resolution is too coarse to resolve individual buildings and shading effects, which significantly influence thermal comfort in urban environments.

The distribution of diurnal urban-rural intensity differences varies across the different urban and land cover zones defined by the LCZs. In the compact urban zones (LCZ 1-3) (figure 4(a)) the distribution is positive

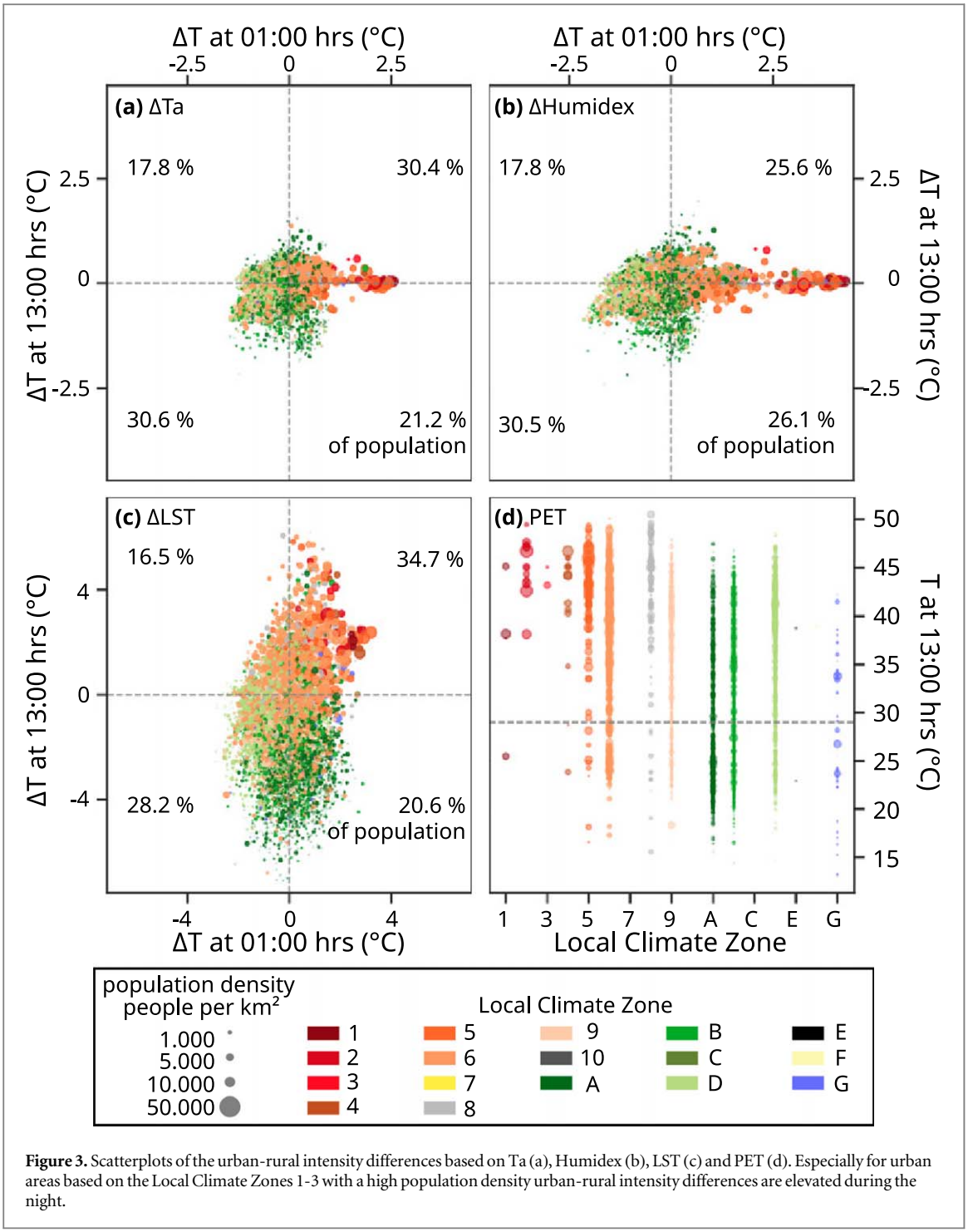

Figure 3. Scatterplots of the urban-rural intensity differences based on Ta (a), Humidex (b), LST (c) and PET (d). Especially for urban areas based on the Local Climate Zones 1-3 with a high population density urban-rural intensity differences are elevated during the night.

skewed, with the Humidex and Ta 90th percentile datasets showing an additional small peak at the higher end of the temperature range. The mean ΔT in these zones are 1.03 ± 0.98 °C (Ta), 1.26 ± 1.09 °C (Ta (90th)), 0.89 ± 1.29 °C (Humidex) with ranges from −0.53 to 2.94 °C (Ta), −0.06 to 3.43 °C (Ta (90th)), −0.88 to 4.17 °C (Humidex). Although these areas can experience cooling, on average, temperatures are higher than the baseline across the three datasets and are susceptible to episodes of extreme heat. In the open urban zones (LCZ 4–6) (figure 4(b)), the temperature distribution is nearly normal, indicating relatively balanced variations throughout the day. The values range from −1.83 °C to 4.33 °C (Humidex), −1.60 °C to 2.81 °C (Ta), and −1.70 °C to 3.30 °C (Ta (90th)) while the mean ΔT for these zones are −0.03 °C ± 0.62 °C (Humidex), −0.00 °C ± 0.48 °C(Ta), and −0.01 °C ±0.56 °C(Ta (90th)). While there are some fluctuations between the urban-rural intensity differences, they are not as extreme as in the compact urban zones. The lower variability also suggests that the microclimates in these zones are more stable, reducing the likelihood of temperature-related stress on the urban population. However, the range of temperatures still indicates the potential for elevated heat stress during the hotter periods of the day. In contrast, the distribution of urban-rural intensity

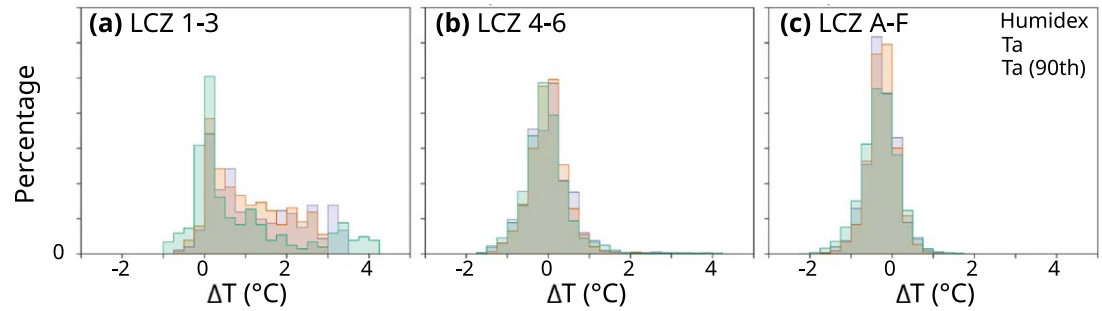

Figure 4. Distribution of diurnal urban-rural intensity differences for compact urban zones (LCZ 1-3) (a) open urban zones (LCZ 4-6) (b) and land cover zones (LCZ A-F) (c) across the datasets Humidex, Ta (mean and 90th percentile).

differences in the land cover type zones (LCZ A-F) (figure 4(c)) exhibit a shift towards colder temperatures compared to baseline. The temperatures range from −2.94 °C to 3.81 °C (Humidex), −2.61 °C to 2.10 °C (Ta), and −2.60 °C to 2.60 °C (Ta 90th) with mean temperatures of −0.30 °C ±0.46 °C (Humidex), −0.24 °C ±0.34 °C (Ta), and −0.28 °C ±0.38 °C (Ta (90th)).

3.2. Temporal development under consideration of LCZs

The temporal development of the UHIs based on the ΔTa dataset follows the expected trend as described by (Stewart and Oke 2012), with urban-rural intensity differences being stronger at night than during the day (figure 5) and with higher positive anomalies for built-type zones, however based on the ΔLST dataset these unique patterns are not as distinguishable. For the ΔTa and ΔHumidex datasets the temporal pattern is similar. The mean of the urban-rural intensity differences of the open and compact urban zones (LCZ 1-6) consistently shows a positive sign with a sinusoidal day-night curve, while other built type zones follow a different, more linear pattern (LCZ 7-10), with land cover type zones (LCZ A-F) forming a slight inverse pattern. Some LCZs, such as Zone 3, have few or no data points (figure S1) and are therefore considered outliers in this analysis. Employing the upper 90th percentile instead of the mean leads to higher positive intensities with longer durations for the open and compact urban zones, while the remaining zones show no discernible differences. The distinction between the LCZs is strongest for the urban-rural intensity differences based on the ΔHumidex. Although the MODIS LST dataset provides only four distinct local overpass times, the overall trend remains observable, showing similar development patterns across all zones.

During the daytime mean urban-rural intensity differences in the compact urban zones are moderate and with minor fluctuations during the day and at nighttime higher with greater variability. In open urban zones, the daytime urban-rural intensity differences are close to the baseline with low variations and at night only slightly elevated (table S2). There is greater variability when considering the upper 90th percentile of Ta.

The percentage of time that urban temperatures exceed rural baseline levels is consistently higher in urban areas (figure 6), with mean values of 3.8 h and 2.8 h of the diurnal cycle for ΔHumidex and ΔTa, respectively, compared to 0.7 h and 0.4 h in rural areas. When considering the Ta 90th percentile, the difference to the ΔHumidex is reduced, with urban areas being hotspots for 3.6 h and rural areas for 0.6 h of the diurnal cycle.

3.3. Comparison between the heat metrics

The Pearson correlation coefficient is calculated between urban-rural intensity differences at night and daytime, excluding PET, for which the direct input parameters are used. The relationship between ΔLST and ΔTa is stronger during the night ($r = 0.43$) compared to the day ($r = 0.24$). This aligns with the understanding that LST and Ta describe different physical properties. During the daytime, a strong positive correlation is observed between ΔLST and PET ($r = 0.49$). For nighttime, since no PET values are available, the correlation is calculated instead between nighttime ΔLST and daytime PET ($r = -0.35$). Additionally, a high positive correlation is found between nighttime ΔLST and ΔHumidex ($r = 0.47$), while the correlation during the daytime is weaker ($r = 0.22$). However, the relationship between these parameters is not constant across all LCZ and varies depending on the specific urban morphology and land cover characteristics of each LCZ (figure S3).

3.4. Heat extremes in the hottest regions of Hesse

To assess the different heat metrics in the context of heat extremes, we first identify the hottest regions in Hesse based on multiple thermal metrics (PET, ΔLST (1:00) using the 90th percentile, ΔHumidex (1:00) using the 90th percentile, hot and very hot days, number of heat wave days and heat wave events) based on a simple ranking score. Using the mean and also the max values per district the district 'City of Frankfurt am Main' (figure

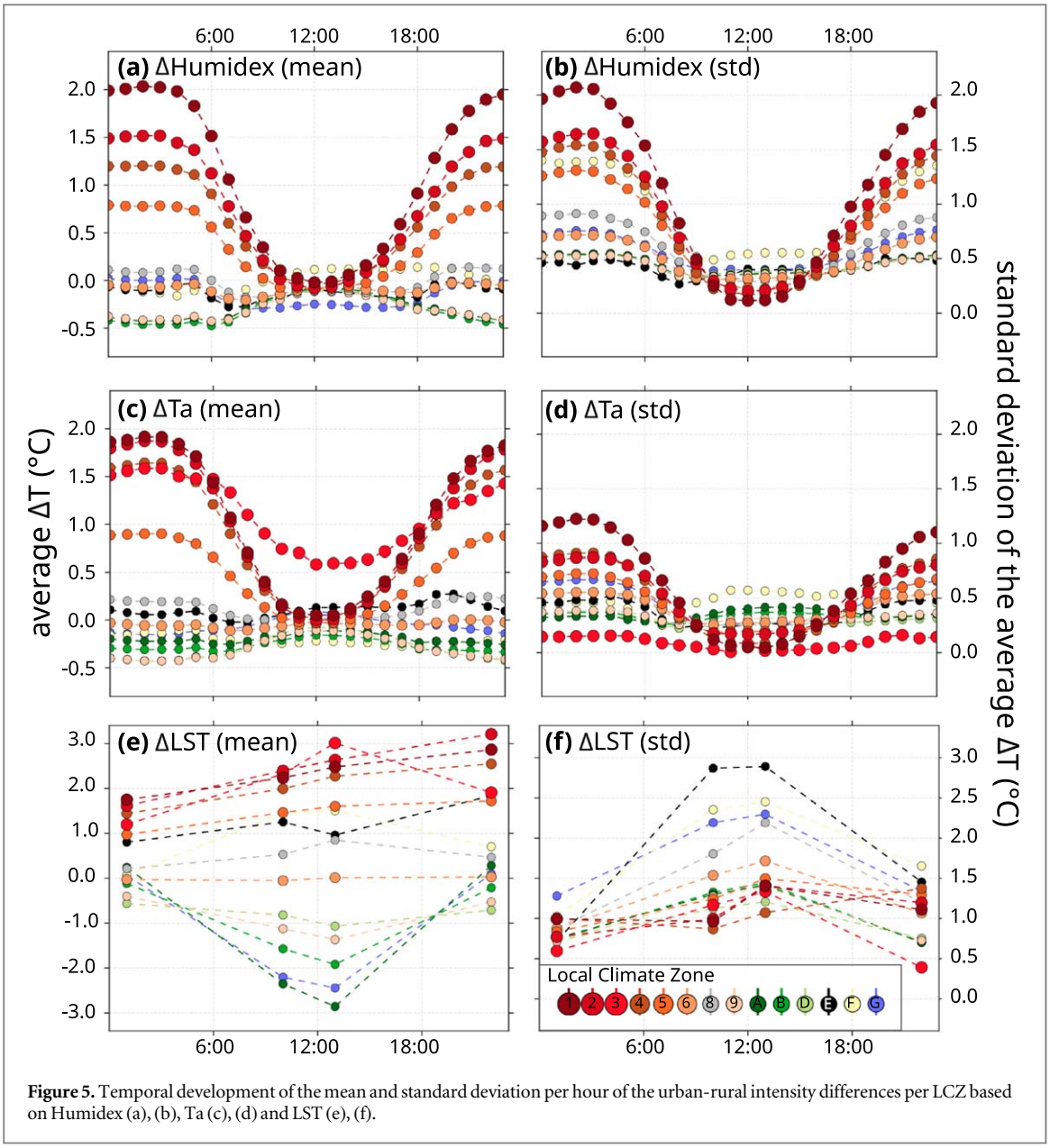

Figure 5. Temporal development of the mean and standard deviation per hour of the urban-rural intensity differences per LCZ based on Humidex (a), (b), Ta (c), (d) and LST (e), (f).

S5) is identified as the hottest region across all analysed parameters. Between 2014 and 2022, the percentage of vulnerable individuals and heat-related emergency deployments increased, indicating a growing risk due to heat (Steul *et al* 2023) within the city. In this district, the strongest correlation with the number of heat wave events and heat wave days is observed in the LST dataset, while the number of (very) hot days aligns most closely with the Humidex dataset (table 1), which is expected, as both parameters are derived from air temperature as a common input variable. With the exception of the PET dataset an urban heat island effect is evident in figure S5. However, for LST and heat waves, the peak values appear to be spatially shifted toward the east.

The correlation analysis for the district 'City of Frankfurt am Main' (table 1) shows a strong relationship between LST anomalies and very hot or hot days, while correlations with heat wave days and events are notably weaker. However, when the focus shifts from just one of the hottest districts to include additional regions with fewer thermal extremes, the relationship weakens (figure 7). This suggests that LST-based metrics are most effective for identifying urban heat hotspots when the area is of high risk of thermal stress. In these cases, LST is a valuable tool for mapping heat-exposed areas. While LST anomalies are effective for identifying localized heat stress like very hot days, they may not fully capture the dynamics of prolonged heat waves when relying on aggregated data. For all analysed parameters, the relationship with the occurrence of (very) hot days is generally stronger than with the occurrence of heat waves, whether considering singular events or cumulative exposure.

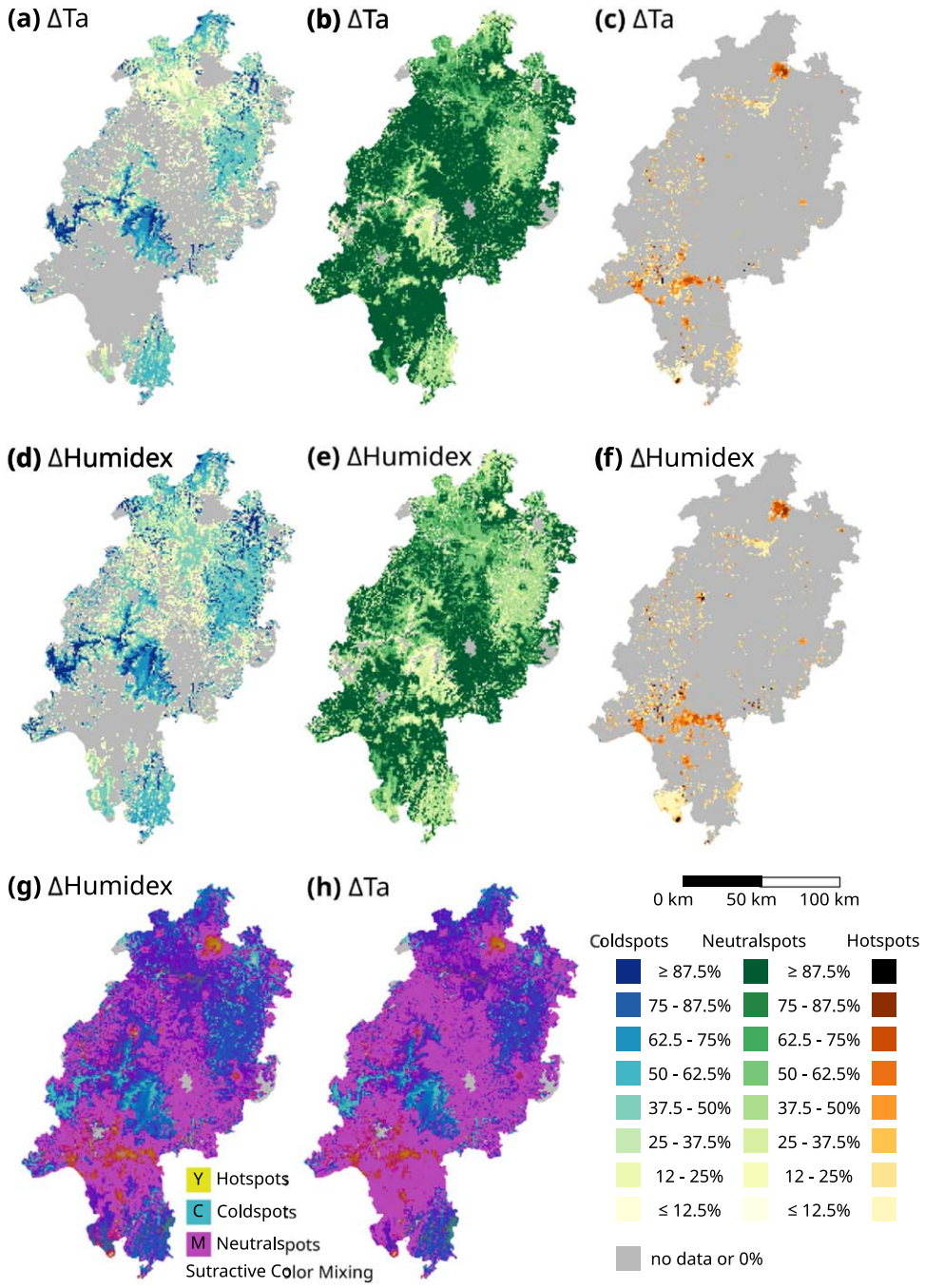

Figure 6. The percentage of time an area is considered colder ($\Delta T < 0.5$) based on ΔTa (a) and ΔHumidex (d) or neutral (ΔT between −0.5 to 0.5) based on ΔTa (b) and ΔHumidex (e) per daily 24 h cycle or hotter ($\Delta T > 0.5$) based on ΔTa (c) and ΔHumidex (f) per daily 24 h cycle. Urban areas (e.g. Kassel and Frankfurt) are hotspots for most of the time of the day based on Ta (h), which are intensified based on the Humidex (g) data.

Table 1. Correlation between heat extreme events and heat parameters such as PET (13:00), ΔLST (90th percentile, 01:00) and ΔHumidex (90th percentile, 01:00). High correlations are found between ΔLST and (very) hot days, but not for heat wave events or days for the district 'City of Frankfurt am Main'.

	PET	Δ_{90th}LST	Δ_{90th}Humidex
heat wave events	−0.07	0.31	0.00
heat wave days	−0.06	0.18	−0.08
very hot days	0.22	0.69	0.95
hot days	0.04	0.69	0.72

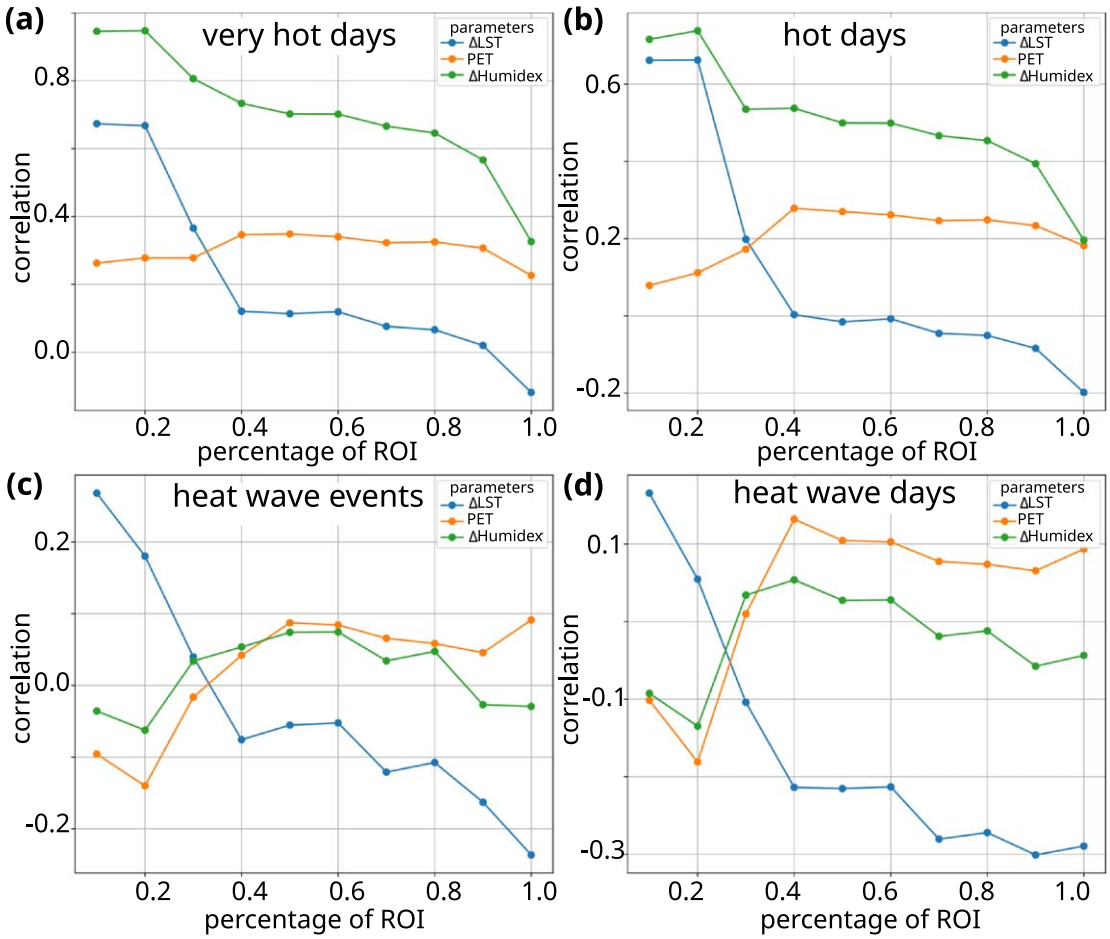

Figure 7. The correlation between temperature metrics—PET (14:00), Δ_{90th}LST (01:00), and Δ_{90th}Humidex (01:00)—and the occurrence of extreme temperature events, including hot days (a), very hot days (b), heat wave events (c), and the number of heat wave days (d), is analysed. The districts are ranked based on their mean temperature extremes score, with each subsequent district added sequentially to the analysed region. The regions ranked as the hottest districts show a stronger correlation with ΔLST, while the relationship weakens as colder regions are included.

4. Discussion

The datasets used in this study differ in terms of data sources and acquisition methods, with unique inherent uncertainties, which complicate direct comparisons and require careful interpretation of results. Although, ideally, datasets should be as comparable as possible, the limited spatiotemporal coverage of heat stress parameters still presents a challenge. A spatial scale of 1 km still represents a relatively low resolution when considering thermal comfort, as it may not fully capture local variations. Although solar radiation is incorporated in the PET model, factors like shading from buildings or vegetation introduce significant variability, making these parameters highly localized and dependent on specific micro-environments. Some LCZ are under represented in this study, therefore an extension to other regions would improve the zone specific results.

An UHI effect based on the thermal comfort index PET dataset can not be observed, however the UHI effect is visible within the Humidex dataset during nighttime, as well as in the Ta and LST datasets. Different thermal comfort indices assign varying weights to the influence of independent variables (Simpson *et al* 2023), and thus the relationship to LST might differ. While the overall spatial pattern of urban-rural intensity differences remains consistent with the inclusion of Humidex, it provides a clearer distinction between urban and rural areas, providing a more detailed and distinct representation of their thermal profiles and properties, though with increased variability. The temporal development of the UHI, based on Ta and Humidex, aligns in general with the description of Stewart *et al* (2021). The characteristic 'spoon shape' is visible in compact and open urban zones (LCZ 1-6), while a linear or inverse spoon pattern emerges in the remaining LCZs. Urban areas experience higher positive urban-rural intensity differences for a longer duration throughout the diurnal cycle with high variability, while land cover zones show a stable and relatively cool temperature profile.

We find, that nearly on third of the population (30.4% (Ta), 25.6% (Humidex), 34.7% (LST)) within Hesse lives in areas with elevated temperatures compared to baseline both during the daytime and the nighttime. Compact urban zones (LCZ 1-3), which already exhibit moderate urban-rural intensity differences during normal conditions, experience higher daytime anomalies during extreme heat conditions. During such events nighttime cooling deficits are prolonged, especially in densely populated built-up zones (LCZs 1-6), although urban-rural intensity differences are consistently exceeding baseline values across all datasets (Ta, Ta 90th percentile, and Humidex) within these areas. Open urban zones (LCZ 4-6) show more balanced and moderate variations throughout the day, indicating that these zones are less prone to extreme temperature fluctuations, although heat stress is still elevated compared to land cover type zones with a low population density. Urban-rural intensity differences during the day are moderate, while nighttime anomalies exhibit high variability. This aligns with the findings of (Iungman *et al* 2024), which show that compact cities in Europe exhibit a stronger UHI effect compared to lower-density cities; although, our analysis focuses on the intra-city level density. However, when analysing the ΔLST dataset, which only captures four specific local overpass times, the patterns are less distinct, particularly in the built-up areas.

Although alternative sources for LST, such as Landsat-8, provide LST at a fine 30 m resolution, its temporal coverage is limited. Nighttime LST is strongly correlated with Ta (Naserikia *et al* 2024), and the nighttime UHI effect is strongest. MODIS offers long-term LST records but at a coarser 1 km resolution. Despite this limitation, it still improves upon the low spatial resolution of geostationary satellites, which prioritize high temporal resolution, capturing diurnal temperature variations more frequently. However, MODIS is restricted to a few observations per day and is dependent on clear-sky conditions, leading to potential data gaps and biases due to cloud cover. Although MODIS Aqua is chosen for its higher likelihood of detecting minimum and maximum temperature deviations (Crosson *et al* 2012), it may not accurately capture the true minimum and maximum temperatures (Sara and Rajasekaran, 2025). While diurnal temperature cycle (DTC) models and spatial downscaling techniques (Lai *et al* 2018, Sara *et al* 2024) can generate high resolution and continuous time-series data, this study focuses on direct observations, as these models can introduce additional uncertainties in urban areas where complex surface heterogeneity and sensor view angles already affect the accuracy of LST products (Trebs *et al* 2021). Future satellite missions, such as the proposed Land Surface Temperature Monitoring (ESA and CEOS 2025) mission by the European Space Agency, could provide higher-resolution and more frequent thermal observations, enhancing the monitoring and analysis of urban heat island effects.

Radiation-related parameters, such as PET and ΔLST, exhibit greater heterogeneity, and their relationship with other heat metrics (ΔLST, ΔTa, ΔHumidex) varies depending on the time of day and urban morphology. Similar to previous studies comparing absolute LST and Ta (Naserikia *et al* 2024), we found lower correlation between ΔLST and both ΔTa and ΔHumidex during the day than during the night. While LST is commonly used to approximate Ta, stronger correlations are found with PET during the day and with ΔHumidex at night. This could be explained by the inclusion of solar radiation in PET, which reflects surface heating influenced by solar radiation (Ghausi *et al* 2023).

Steul *et al* (2018) demonstrated a link between heat wave duration and excess mortality, suggesting that duration is a better indicator of excess mortality than temperature alone during heat waves in Frankfurt. However, our analysis found a weak correlation between the analysed parameters and heat wave days and events, while the relationship with (very) hot days was slightly stronger. Although Agathangelidis *et al* (2022) found an increasing correlation between LST and the progressing heatwaves in our temporally aggregated data, this pattern is not evident. Instead, we observe a slightly higher correlation between LST and the number of heatwave events in Frankfurt compared to the correlation with the number of heatwave days, although this trend is not consistently observed across all regions. This aligns more with the the findings of Sara and Rajasekaran (2025), who found that the coarse resolution of about 1 km LST is not capable of capturing the effects of heat waves, whereas the application of DTC modelling allows the generation of high resolution LST, making it suitable for identifying heat wave effects. This highlights the need to incorporate additional factors to more accurately assess prolonged heat wave risks, rather than relying solely on coarse resolution LST. Nevertheless, in areas experiencing high temperature stress, LST-based metrics serve as a useful proxy for identifying urban heat hotspots, making them valuable for mapping heat-exposed areas and informing mitigation strategies.

While LCZ classification and census-based population density provide a baseline for heat exposure risk, they overlook human mobility and urban function. Commuting patterns and daily activities influence actual exposure, requiring a more dynamic assessment. Thermal comfort metrics based on population averages fail to account for vulnerable groups such as the elderly and children (Wallenberg *et al* 2023), whose spatial distribution, near schools or nursing homes, affects risk. Since thermal comfort is influenced by personal factors (such as clothing or activity level) as well as environmental factors (such as shading from solar radiation), both aspects should be considered for climate adaptation. Additionally, higher temperatures in compact, high-density cities intensify UHI effects and elevate air pollution levels, exacerbating mortality risks (Iungman *et al* 2024). When considering human health in climate change scenarios, indirect effects must also be taken into

account. Future studies should therefore also focus on the inclusion of urban form, demographics, and multi-hazard interactions for effective heat mitigation and adaptation strategies.

5. Conclusion

In this study we focus on urban-rural intensity differences for the comparison of LST, Ta, and the thermal comfort metrics PET and Humidex. The analysis is conducted for the region of Hesse, Germany, at a spatial resolution of 1 km over a full decade (2011-2022), using hourly averages or the 90th percentile of the available data from the summer months June, July and August.

Our results indicate that, although LST is commonly used to approximate Ta, it has limitations in capturing the distinct patterns between the LCZs and its correlation with Ta is generally weaker during the daytime compared to nighttime. Higher correlations are observed with PET during the day and with ΔHumidex at night, as well as with (very) hot days, whereas the association with the location and duration of heat wave events remains weak. This indicates that while LST anomalies are effective for identifying localized heat stress, they may not fully capture the dynamics of prolonged heat waves when relying on aggregated data. The inclusion of RH in the form of ΔHumidex allows for clearer distinctions between the LCZs than on ΔTa alone and additionally shows a magnification of the UHI effect for densely built up areas. Relying solely on LST or Ta may underestimate the heat stress experienced by urban populations. This is crucial since nearly one third of the population in Hesse lives in areas with elevated temperatures both during the daytime and at night compared to baseline temperature. Especially the population in compact urban zones (LCZ 1-3) experiences high urban-rural intensity differences, with prolonged nighttime cooling deficits, while open urban zones (LCZ 4-6) exhibit more moderate heat stress but still show elevated nighttime anomalies.

Future studies should integrate urban form, demographics, and multi-hazard interactions with socioeconomic data to identify vulnerable populations. Combining these data with heat parameters could provide a more comprehensive understanding of heat stress distribution, essential for the targeted implementation of heat mitigation strategies.

Acknowledgments

We acknowledge support from the Karlsruhe Institute of Technology (KIT) Publication Fund of the Karlsruhe Institute of Technology. Susanne A. Benz is supported by a Freigeist Fellowship, funded by the Volkswagen Foundation. Svea Krikau is supported by the Center for Disaster Management and Risk Reduction Technology (CEDIM) at KIT. Special thanks go to Natalie Scheck for the access to the thermal comfort dataset PET.

Data availability statement

The data supporting the results of this study are openly available under the following DOI: https://doi.org/10.5281/zenodo.14592191 (Krikau 2025).

ORCID iDs

S Krikau https://orcid.org/0009-0000-5723-9627
S A Benz https://orcid.org/0000-0002-6092-5713

References

Adinolfi M, Raffa M, Reder A and Mercogliano P 2023 Investigation on potential and limitations of ERA5 Reanalysis downscaled on Italy by a convection-permitting model *Clim. Dyn.* **61** 4319–42

Agathangelidis I, Cartalis C, Polydoros A, Mavrakou T and Philippopoulos K 2022 Can satellite-based thermal anomalies be indicative of heatwaves? An investigation for MODIS land surface temperatures in the mediterranean region *Remote Sensing* **14** 3139

Ämter des Bundes A and und der Länder S 2011 INSPIRE Dataset Feed: Zensusatlas 2011—Bundesweite kleinräumige Daten (1 km2-Raster) der amtlichen Statistik zu Bevölkerung, Gebäude und Wohnungen available at https://geoportal.de/Info/dd0e9318-0fa9-4226-b61b-e9b0e4b04b9b (accessed: 2024-08-20)

Beck H E, Zimmermann N E, McVicar T R, Vergopolan N, Berg A and Wood E F 2018 Present and future Köppen-Geiger climate classification maps at 1-km resolution *Scientific Data* **5** 180214

Beck H E, Zimmermann N E, McVicar T R, Vergopolan N, Berg A, Berg A and Wood E F 2020 Publisher Correction: Present and future Köppen-Geiger climate classification maps at 1-km resolution *Scientific Data* **7** 274

Benz S A, Davis S J and Burney J A 2021 Drivers and projections of global surface temperature anomalies at the local scale *Environ. Res. Lett.* **16** 064093

Blazejczyk K, Epstein Y, Jendritzky G, Staiger H and Tinz B 2012 Comparison of UTCI to selected thermal indices *Int. J. Biometeorol.* **56** 515–35
Cetin M, Ozenen Kavlak M, Senyel Kurkcuoglu M A, Bilge Ozturk G, Cabuk S N and Cabuk A 2024 Determination of land surface temperature and urban heat island effects with remote sensing capabilities: the case of Kayseri Türkiye *Nat. Hazards* **120** 5509–36
Chakraborty T and Lee X 2019 A simplified urban-extent algorithm to characterize surface urban heat islands on a global scale and examine vegetation control on their spatiotemporal variability *Int. J. Appl. Earth Obs. Geoinf.* **74** 269–80
Coccolo S, Kämpf J, Scartezzini J L and Pearlmutter D Outdoor human comfort and thermal stress: a comprehensive review on models and standards *Urban Climate* **18** 3357
Coutts A M, Harris R J, Phan T, Livesley S J, Williams N S G and Tapper N J 2016 Thermal infrared remote sensing of urban heat: Hotspots, vegetation, and an assessment of techniques for use in urban planning *Remote Sens. Environ.* **186** 637–51
Crosson W L, Al-Hamdan M Z, Hemmings S N and Wade G M 2012 A daily merged MODIS Aqua-Terra land surface temperature data set for the conterminous United States *Remote Sens. Environ.* **119** 315–24
Demuzere M, Kittner J, Martilli A, Mills G, Moede C, Stewart I D, van Vliet J and andBechtel B 2022 A global map of local climate zones to support earth system modelling and urban-scale environmental science *Earth System Science Data* **14** 3835–73
Deutscher Wetter Dienst D 2025 Wetter und Klima Explanations - Hot days available at https://www.dwd.de/EN/ourservices/germanclimateatlas/explanations/elements/_functions/faqkarussel/heissetage.html (accessed: 2025-02-26)
Di Napoli C, Hogan R J and Pappenberger F 2020 Mean radiant temperature from global-scale numerical weather prediction models *Int. J. Biometeorol.* **64** 1233–45
Diem P K, Nguyen C T, Diem N K, Diep N T H, Thao P T B, Hong T G and Phan T N 2024 Remote sensing for urban heat island research: progress, current issues, and perspectives *Remote Sensing Applications: Society and Environment* **33** 101081
ESA and CEOS 2025 Sentinel LSTM-A satellite mission summary | CEOS database available at https://database.eohandbook.com/database/missionsummary.aspx?missionID=1041(accessed: 2025-03-17)
European Environment Agency May 2020 CORINE Land Cover 2018 (raster 100 m), Europe, 6-yearly - version 2020_20u1 10.2909/960998C1-1870-4E82-8051-6485205EBBAC
Fiala D, Lomas K J and Stohrer M 2001 Computer prediction of human thermoregulatory and temperature responses to a wide range of environmental conditions *Int. J. Biometeorol.* **45** 143–59
Fuladlu K 2022 Thermal response to land-use land-cover patterns: an experimental study in famagusta, cyprus *CLEAN - Soil, Air, Water* **50** 2100284
Ghausi S A, Tian Y, Zehe E and Kleidon A 2023 Radiative controls by clouds and thermodynamics shape surface temperatures and turbulent fluxes over land *Proc. Natl Acad. Sci.* **120** e2220400120
Hajat S, O'Connor M and Kosatsky T 2010 Health effects of hot weather: from awareness of risk factors to effective health protection *The Lancet* **375** 856–63
Höppe P 1999 The physiological equivalent temperature - a universal index for the biometeorological assessment of the thermal environment *Int. J. Biometeorol.* **43** 71–5
Imran H M, Hossain A, Shammas M I, Das M K, Islam M R, Rahman K and Almazroui M 2022 Land surface temperature and human thermal comfort responses to land use dynamics in Chittagong city of Bangladesh *Geomatics, Natural Hazards and Risk* **13** 2283–312
IPCC 2023 Climate Change 2023: Synthesis Report. *Contribution of Working Groups I, II and III to the Sixth Assessment Report of the Intergovernmental Panel on Climate Change (IPCC)* IPCC Geneva, Switzerland 35–115 [Core Writing Team, H. Lee and J. Romero (eds.)]
Iungman T, Khomenko S, Barboza E P, Cirach M, Gonçalves K, Petrone P, Erbertseder T, Taubenböck H, Chakraborty T and Nieuwenhuijsen M 2024 The impact of urban configuration types on urban heat islands, air pollution, CO_2 emissions, and mortality in Europe: a data science approach *The Lancet Planetary Health* **8** e489–505
Jendritzky G, de Dear R and Havenith G 2012 UTCI–why another thermal index? *Int. J. Biometeorol.* **56** 421–8
Karimi A, Mohammad P, Gachkar S, Gachkar D, Garcìa-Martìnez A, Moreno-Rangel D and Brown R D 2021 Surface urban heat island assessment of a cold desert city: a case study over the isfahan metropolitan area of Iran *Atmosphere* **12** 1368
Kariminia S, Shamshirband S, Motamedi S, Hashim R and Roy C 2016 A systematic extreme learning machine approach to analyze visitors thermal comfort at a public urban space *Renew. Sustain. Energy Rev.* **58** 751–60
Karlsruhe S 2024 Wetterdaten Projekt CityClim avaiable at https://transparenz.karlsruhe.de/dataset/sensordaten-projekt-cityclim (accessed: 2024-12-15)
Ketterer C, Nielinger J, Hasel M and Röckle R 2022 *Erstellung einer landesweiten Klimaanalyse/ Kaltluftströmungssituation unter Berücksichtigung des klimawandelbedingten Temperaturanstiegs Abschlussbericht Hessisches Ministerium für Wirtschaft, Energie, Verkehr und Wohnen* https://landesplanung.hessen.de/sites/landesplanung.hessen.de/files/2022-08/landesweiteklimaanalysehessen_abschlussbericht_20220531.pdf
Krähenmann S, Walter A, Brienen S, Imbery F and Matzarakis A 2018 High-resolution grids of hourly meteorological variables for Germany *Theor. Appl. Climatol.* **131** 899–926
Krikau S 2025 Spatio-Temporal Analysis of Heat Extremes *Zenodo* https://doi.org/10.5281/zenodo.14592191
Lai J, Zhan W, Huang F, Voogt J, Bechtel B, Allen M, Peng S, Hong F, Liu Y and Du P 2018 Identification of typical diurnal patterns for clear-sky climatology of surface urban heat islands *Remote Sens. Environ.* **217** 203–20
Li J *et al* 2023 Satellite-based ranking of the world's hottest and coldest cities reveals inequitable distribution of temperature extremes *Bull. Am. Meteorol. Soc.* **104** E1268–81
Lin J, Wei K and Guan Z 2024 Exploring the connection between morphological characteristic of built-up areas and surface heat islands based on MSPA *Urban Climate* **53** 101764
Masterton J M and Richardson F A 1979 Humidex: A method of quantifying human discomfort due to excessive heat and humidity *CLI; 1-79* En57-23/1-79E-PDF Environment Canada, Atmospheric Environment Service iii, 45 p. Digitized edition from print publications. gc.ca/pub?id=9.865813&sl=1
Mavrakou T, Polydoros A, Cartalis C and Santamouris M 2018 Recognition of thermal hot and cold spots in urban areas in support of mitigation plans to counteract overheating: application for athens *Climate* **6** 16 Number: 1 Publisher: Multidisciplinary Digital Publishing Institute
Meehl G A and Tebaldi C 2004 More Intense, More Frequent, and Longer Lasting Heat Waves in the 21st Century *Science* **305** (5686) 994–7
Migliari M, Babut R, De Gaulmyn C, Chesne L and Baverel O 2022 The Metamatrix of Thermal Comfort: A compendious graphical methodology for appropriate selection of outdoor thermal comfort indices and thermo-physiological models for human-biometeorology research and urban planning *Sustainable Cities and Society* **81** 103852
Mora C *et al* 2017 Global risk of deadly heat *Nat. Clim. Change* **7** 501–6

Naserikia M, Hart M A, Nazarian N, Bechtel B, Lipson M and Nice K A 2023 Land surface and air temperature dynamics: The role of urban form and seasonality *Science of The Total Environment* **905** 167306
Naserikia M, Nazarian N, Hart M A, Sismanidis P, Kittner J and Bechtel B 2024 Multi-city analysis of satellite surface temperature compared to crowdsourced air temperature *Environ. Res. Lett.* **19** 124063
Nogueira M, Hurduc A, Ermida S, Lima D C A, Soares P M M, Johannsen F and Dutra E 2022 Assessment of the Paris urban heat island in ERA5 and offline SURFEX-TEB (v8.1) simulations using the METEOSAT land surface temperature product *Geoscientific Model Development* **15** 5949–65
Oke T R 1973 City size and the urban heat island *Atmospheric Environment (1967)* **7** 769–79
Patel S, Indraganti M and Jawarneh R N 2024 A comprehensive systematic review: Impact of Land Use/ Land Cover (LULC) on Land Surface Temperatures (LST) and outdoor thermal comfort *Build. Environ.* **249** 111130
Pena Acosta M, Vahdatikhaki F, Santos J and Dorée A G 2023 A comparative analysis of surface and canopy layer urban heat island at the micro level using a data-driven approach *Sustainable Cities and Society* **99** 104944
Raymond C, Matthews T and Horton R M 2020 The emergence of heat and humidity too severe for human tolerance *Science Advances* **6** eaaw1838
Roy A, Rajasekaran E, Harod R and andGnanappazham L 2024 Land surface temperature anomalies as indicators of urban land cover change —a study of two indian cities *Earth Science, Systems and Society* **4** 10096
Rød J K and Maarse M J 2021 Using citizen sensing to identify heat-exposed neighbourhoods *Urban Science* **5** 14
Sara K and Rajasekaran E 2025 High spatiotemporal resolution land surface temperature reveals fine-scale hotspots during heatwave events over India *Environ. Res. Commun.* **7** 035027
Sara K *et al* 2024 Combining spatial downscaling techniques and diurnal temperature cycle modelling to estimate diurnal patterns of land surface temperature at field scale *PFG -Journal of Photogrammetry, Remote Sensing and Geoinformation Science* **92** 723–40
Semenza J C, Rubin C H, Falter K H, Selanikio J D, Flanders W D, Howe H L and Wilhelm J L 1996 Heat-related deaths during the July 1995 heat wave in Chicago *New Engl. J. Med.* **335** 84–90
Simpson C H, Brousse O, Ebi K L and Heaviside C 2023 Commonly used indices disagree about the effect of moisture on heat stress *npj Climate and AtmosphericScience* **6** 1–7
Sismanidis P, Bechtel B, Keramitsoglou I, Liu Z and Zhan W 2023 The Intensity of Surface Urban Heat Islands in the Global North during the COVID-19 Lockdowns *2023 Joint Urban Remote Sensing Event (JURSE) (Heraklion, Greece)* 1–4
Speak A F and Salbitano F 2022 Summer thermal comfort of pedestrians in diverse urban settings: a mobile study *Build. Environ.* **208** 108600
Steul K, Kowall B, Oberndörfer D, Domann E and Heudorf U 2023 Rescue service deployment data as an indicator of heat morbidity in Frankfurt / Main, Germany (2014-2022) - Trend association with various heat exposure indicators and considerations for outreach *International Journal of Hygiene andEnvironmental Health* **254** 114250
Steul K, Schade M and Heudorf U 2018 Mortality during heatwaves 2003-2015 in Frankfurt-Main - the 2003 heatwave and its implications *InternationalJournal of Hygiene and Environmental Health* **221** 81–6
Stewart I D, Krayenhoff E S, Voogt J A, Lachapelle J A, Allen M A and Broadbent A M 2021 Time evolution of the surface urban heat island *Earth's Future* **9** e2021EF002178
Stewart I D and Oke T R 2012 Local climate zones for urban temperature studies *Bull. Am. Meteorol. Soc.* **93** 1879–900
Stone B J *et al* 2023 How blackouts during heat waves amplify mortality and morbidity risk *Environmental Science & Technology* **57** 8245–55
Tartarini F and Schiavon S 2020 pythermalcomfort: a Python package for thermal comfort research *Software* X **12** 100578
Trebs I *et al* 2021 The role of aerodynamic resistance in thermal remote sensing-based evapotranspiration models *Remote Sens. Environ.* **264** 112602
Venter Z S, Chakraborty T and Lee X 2021 Crowdsourced air temperatures contrast satellite measures of the urban heat island and its mechanisms *Science Advances* **7** eabb9569
Voogt J A and Oke T R 2003 Thermal remote sensing of urban climates *Remote Sens. Environ.* **86** 370–84
Wallenberg N, Rayner D, Lindberg F and Thorsson S 2023 Present and future heat stress of preschoolers in five Swedish cities *Climate Risk Management* **40** 100508
Walther E and Goestchel Q 2018 The P.E.T. comfort index: Questioning the model *Build. Environ.* **137** 1–10
Wan Z, Hook S and Hulley G 2015 MOD11A1 MODIS/Terra Land Surface Temperature/Emissivity Daily L3 Global 1km SIN Grid V006 *NASA EOSDIS Land Processes Distributed Active Archive Center*
Wan Z, Hook S and Hulley G 2021 MODIS/Aqua Land Surface Temperature/Emissivity Daily L3 Global 1 km SIN Grid V061 *NASA EOSDIS Land Processes Distributed Active Archive Center* 10.5067/MODIS/MYD11A1.061
Wang C, Zhan W, Li L, Wang S, Wang C, Miao S, Du H, Jiang L and Jiang S 2023 Urban heat islands characterized by six thermal indicators *Build. Environ.* **244** 110820
Xu D, Wang Y, Zhou D, Wang Y, Zhang Q and Yang Y 2024 Influences of urban spatial factors on surface urban heat island effect and its spatial heterogeneity: a case study of Xi'an *Build. Environ.* **248** 111072
Yadav N, Rajendra K, Awasthi A, Singh C and Bhushan B 2023 Systematic exploration of heat wave impact on mortality and urban heat island: a review from 2000 to 2022, 2022 *Urban Climate* **51** 101622
Zare S, Hasheminejad N, Shirvan H E, Hemmatjo R, Sarebanzadeh K and Ahmadi S 2018 Comparing universal thermal climate index (UTCI) with selected thermal indices/environmental parameters during 12 months of the year *Weather and Climate Extremes* **19** 49–57